Lawrence Berkeley National Laboratory

Title
A slice of an aluminum particle: Examining grains, strain and reactivity

Permalink
https://escholarship.org/uc/item/3gp8s2m5

Authors
McCollum, Jena
Smith, Dylan K
Hill, Kevin J
et al.

Publication Date
2016-11-01

DOI
10.1016/j.combustflame.2016.09.002

Peer reviewed

A Slice of an Aluminum Particle: Examining Grains, Strain and Reactivity

Jena McCollum[1], Dylan K. Smith[1], Kevin J. Hill[1], Michelle L. Pantoya[1*], Juliusz Warzywoda[2], Nobumichi Tamura[3]

[1] *Mechanical Engineering Department, Texas Tech University, Lubbock, TX 79409*

[2] *Materials Characterization Center, Whitacre College of Engineering, Texas Tech University, Lubbock, TX 79409*

[3] *Advanced Light Source, Lawrence Berkeley National Laboratory, Berkeley, CA 94720*

*Corresponding author contact information: Email: michelle.pantoya@ttu.edu; Phone: 806-834-3733

Abstract

Micron-scale aluminum (Al) particles are plagued by incomplete combustion that inhibits their reactivity. One approach to improving reactivity is to anneal Al particles to increase dilatational (volumetric) strain which has also been linked to increased combustion performance. While optimal annealing temperatures have been identified (roughly 300 °C), little is known about cooling rate effects on particle combustion performance. This study examines the effect of quenching after annealing Al microparticles to 100, 200 and 300 °C on intra-particle dilatational strain and reactivity. Synchrotron X-ray diffraction analysis of the particles reveals the cooling rates in the range from 0.007 to 0.38 K/s have little effect on the dilatational strain of the aluminum-core, alumina-shell particles. The annealed and quenched Al particles were then combined with a metal oxidizer (copper oxide) to examine reactivity. Flame propagation experiments follow the same trend: flame speeds are unchanged until a critical annealing temperature of 300 °C is reached and performance is maintained for each annealing temperature regardless of cooling rate. These results show that altering the mechanical properties and combustion performance of Al particles is strongly dependent on the annealing temperature and unchanged with variation in cooling rate. The contributions from elastic and plastic deformation mechanisms on strain are also considered and additional experimental results are shown on the microstructure of an Al particle. Focused ion beam milling of an Al particle to electron transparency was combined with transmission electron microscope imaging in order to examine the microstructure of the Al particles. This confirmed that the Al microparticles have a polycrystalline structure shown by grains all exceeding 100 nm in size.

Key Words: aluminum, annealing, quenching, combustion, pre-stress, synchrotron XRD, FIB, TEM, powder metallurgy

Introduction

The highly exothermic nature of thermite reactions enables their use in a variety of energy generating applications such as material processing [1–3], welding and joining[4,5], and alloying [6,7]. This reaction occurs by oxygen transfer between a metal fuel (i.e., aluminum, Al) and metal oxide (i.e., copper oxide, CuO). Recent advances in particle production techniques have brought fuel particle sizes down to the nano-scale, and many have shown that Al nanoparticles (nAl) exhibit higher reactivity than Al microparticles (µAl). There are several potential mechanisms explaining the increase in reactivity for nAl [8–16]. However, interest is now shifting towards utilizing what is understood about the mechanisms promoting optimal reactivity in nAl particles towards engineering more reactive µAl particles. This is because µAl particles are lower in cost and do not possess the intrinsic health and environmental risks that exist with their nano-scale counterparts. So, a common goal motivating Al particle combustion research is to understand what mechanistically controls increased reactivity at the nano-scale and exploit these parameters by designing µAl particles to that exhibit nAl particle-like reactivity.

One option is to subject Al powders to a series of thermal treatments to purposefully alter mechanical properties on a single particle level. This work began with Dikici et al. who annealed µAl or nAl mixed with molybdenum trioxide (MoO_3) [17]. They showed that the combustion performance was dependent on annealing temperature (105 and 170 °C) and quench rate (0.06 and 0.13 °C/s) for both nAl and µAl. However novel this approach was toward enhancing Al reactivity, consistent and direct correlations between particle size, annealing temperature and cooling rate were not established and not well understood. Further investigation by Levitas et al. focused on µAl and CuO [18]. These composites were heated to a variety of annealing temperatures (110, 145, 170 and 200 °C) and quenched at three different rates (0.06,

0.16 and 0.46 °C). The combustion performance increased with higher annealing temperatures

for all cooling rates except for the lowest cooling rate at the highest two annealing temperatures.

The lower performance associated with the slowly quenched mixture may be attributed to low

temperature surface chemistry reactions (i.e., reactive sintering) between Al and CuO which has

been reported by others [19]. However, with fast quenching, these composites still showed

increased flame speed when annealed to 170 and 200 °C. This implies that although there are

likely surface reactions during thermal treatment for mixed powder, pre-stressing particles is still

feasible for increasing µAl performance.

To gain a better understanding of the effects of annealing µAl particles separately from

annealing composites, McCollum et al. subjected µAl to a variety of thermal treatments (100,

200 and 300 °C) with one quench rate [20]. The Al was then combined with CuO after thermal

treatment to assess reactivity. They found that energy propagation for the 100 and 200 °C

treatments did not significantly differ from the untreated case, but the 300 °C treatment showed

an increase in energy propagation by 24% [20]. These findings were coupled with synchrotron

X-ray diffraction (XRD) measurements to quantify particle strain. The strain response was

unchanged for the µAl annealed to 100 and 200 °C compared to the untreated particles. The

average strain for µAl annealed to 300 °C increased by 660% [20]!

Others also studied annealing and quenching µAl particles in order to observe changes in

mechanical properties [21, 22]. Bachmaier and Pippan [21] and Abdoli et al. [22] found that

when consolidating pre-stressed powder into a bulk material, changes occurring on the particle

level affected the mechanical properties of the final bulk material. The onset for mechanical

change for both studies was similar and occurred above 200 °C; and may be due to the high

purity of the aluminum particles used [20, 21].

In terms of combustion performance, these results are consistent with what was previously observed for increased reactivity corresponding with increased annealing temperature [20]. However, the role of quench rate in µAl reactivity is still not clear because previous studies involving quenching were performed on composites such that reactive sintering may have masked other behaviors. This study investigates the role of quenching rate on increasing (or decreasing) µAl reactivity, measured in terms of flame speed. Also, the mechanism responsible for changes in dilatational strain are considered because of the indirect relationship between flame speed and strain. Towards this end, Al particles are dissected to resolve grain size and polycrystalline microstructure. To the authors' knowledge, the polycrystalline microstructure of a µAl particle has not been visualized previously.

Experimental

Sample Preparation

Aluminum particles were procured from Alfa Aesar (Ward Hill, MA). Average particle diameter was measured using an AccuSizer 780 optical particle size analyzer (Santa Barbara, CA). The untreated Al particles have an average diameter of 5 µm and their size distribution is shown in Supplementary Information section, **Fig. S1a**. The size distributions for the annealed and quenched Al particles are presented in **Fig. S1b-d** and show negligible change after thermal treatment from that of the untreated Al particles.

Aluminum particles (200 mg) were loaded into ceramic trays and subjected to various annealing temperatures and quenched to room temperature. This process used a Neytech Qex vacuum oven (Torrance, CA). This is a programmable oven such that the powder was annealed to 100, 200 or 300°C at a controlled rate of 10 Kelvin per minute (KPM) and held at the

prescribed temperature for 15 minutes. Post-heating, the Al powder designated as "slow cooled"

reached room temperature by leaving the oven in the closed position and allowing the entire

system to cool by natural convection. The Al powder that was cooled fast was removed from the

oven post-heating and placed in a refrigeration unit until the powder reached room temperature.

Each thermal cycle was monitored using an InstruNet Direct to Sensor system (Charlestown,

MA) and Type K thermocouples from Omega Engineering (Stamford, CT). Aluminum powder

temperature response as a function of time is shown in the Supplementary Information section as

Fig. S2. Materials cool according to a lump capacitance model due to the natural convection

conditions (see Supplementary Information for detailed lump capacitance analysis). In both

cooling cases, the temperature evolution reduces exponentially and experimental results are

approximated by Equation (1).

$$T = T_a + (T_0 - T_a) \exp(-At) \text{ with } A_1 = 0.0078 \text{ s}^{-1} \quad \text{and } A_2 = 0.00025 \text{ s}^{-1} \tag{1}$$

In Equation (1), T_a is ambient temperature, T_0 is annealing temperature, t is time and A_1 (fast

cooling) and A_2 (slow cooling) are determined by examining the exponential plots of the cooling

curves and identifying the coefficient. An average quenching rate ranges from 0.13 to 0.38 K·s^{-1}

for fast cooling and 0.007 to 0.014 K·s^{-1} for slow cooling. Note that differences in average

cooling rates are present due to variations in annealing temperature. Note also that while these

quench rates vary by an order of magnitude, both are relatively slow for traditional quenching

treatments in metallurgy.

Post-treatment, Al particles were mixed with 50 nm average particle diameter spherical

CuO particles (Sigma Aldrich; St. Louis, MO) to an equivalence ratio of 1.2 (i.e., slightly fuel

rich). The dry powders were weighed and suspended in isopropanol and mixed using a Misonix

Sonicator 3000 probe for 2 minutes. The suspensions were poured into a Pyrex dish and

isopropanol evaporated in a fume hood for 24 hours. The dry powders were retrieved and sieved to break up large agglomerations.

The powders were carefully loaded into 3 mm inner diameter, 8 mm outer diameter, 10 cm long quartz tubes, each containing 750 mg of powder. The theoretical maximum density (TMD) of the loose powder was determined by a weighted average of the bulk densities of Al (2.7 g·cm^{-3}), Al$_2$O$_3$ (3.95 g·cm^{-3}), and CuO (6.31 g·cm^{-3}) and calculated to be 5.53 g·cm^{-3}. The measured bulk density was 1.06 g·cm^{-3} such that tubes were loaded to 19.2% TMD. A detailed explanation with calculations for the determination of bulk density and % TMD is provided in Supplementary Information.

Strain Measurements

X-ray diffraction (XRD) experiments were performed at the Advanced Light Source facility at Lawrence Berkeley National Laboratory on beamline 12.3.2 using a micron focused synchrotron X-ray beam. Aluminum powder was spread over glass slides and scanned under the X-ray beam (either polychromatic or monochromatic) while a diffraction pattern was collected at each step using a DECTRIS Pilatus 1 M detector. The measured relative small shifts in the reflection positions in the Laue pattern provides the deviatoric strain tensor of the material while the measurement of the energy of one reflection provides the dilatational component. Data were processed using XMAS software [23]. The beamline experimental setup and capabilities have been described elsewhere [24].

Flame Speed Measurements

The apparatus and procedure for loading powder filled tubes and measuring flame speeds are described in more detail elsewhere [20, 25] but summarized here. Both ends of a quartz 10

cm long and 3 mm inside diameter tube were sealed with one side securing a length of nickel-chromium wire for ignition. Ten experiments per annealing temperature were performed to establish repeatability. Each tube was placed inside a blast chamber for ignition and flame propagation experiments. The powders were ignited and flame propagation was observed through a viewing window in the chamber. The reaction was recorded with a Phantom v7 (Vision Research, Wayne, NJ) high speed camera at a rate of 29,000 frames per second and 512 x 128 resolution. The camera was aligned perpendicular to the direction of flame propagation. Flame speed was determined by tracking the flame front through a referenced time and distance using the Vision Research Software. The resolution of the flame speed for this diagnostic is 0.1 $m \cdot s^{-1}$. The largest source of uncertainty in the measurement is due to repeatability and is shown for each data set in the results.

Coincidence of Synchrotron XRD and Flame Speed Measurements

It is important to note that there may be aging effects on the Al particles that are thermally treated [26]. For this reason, the timing for the synchrotron XRD and flame speed measurements was coordinated such that both measurements were made on material aged for the same duration upon thermal treatment. In the results reported here for synchrotron XRD and flame speed, all powders were aged 28 days from thermal treatment to experimental measurements.

Focused Ion Beam (FIB) Cross-sectioning and TEM Lattice Imaging

Most theoretical work focuses on the hydrostatic mean stress component of the internal stresses in an Al particle that are due to interaction between the core and shell. However, insight into the microstructure of grains may also provide an understanding of other mechanical properties such as hardness, which may also impact reactivity [26]. There are reports of modifications to

grain size in Al particles that result from annealing and quenching [21, 22]. However, visualizing the grains, grain boundaries, and grain distributions within an individual Al particle has not previously been reported. There are predictions that in nano-scale Al particles, the core is not composed of grains but is rather a single crystal. Particles smaller than 25 µm in diameter are synthesized in the same manner as nanoparticles using methods that include atomization and wire explosion. One goal of this work was to identify the grain microstructure within the core of a 10 µm diameter particle. Stresses due to heterogeneities within the core of the Al particle can occur at grain boundaries and are dependent on grain size.

Micron-scale Al particles cannot be analyzed for the grain structure with a transmission electron microscope (TEM) without prior size reduction. Due to size constraints with typical TEM imaging, µAl particles were thinned to ~100 nm cross sections using a Hitachi NB5000 focused ion & electron beam (dual-beam FIB-SEM) system. First, Al particles ~10 µm in diameter were coated with a protective carbon layer then a protective tungsten layer. This allowed the gallium ion beam to prepare micro-samples from Al particles, lift out these micro-samples from the substrate, and then thin the micro-samples without damage. After coating, the Al particles were pre-thinned to form ~5 µm thick micro-samples. The micro-samples were first attached to a tungsten probe via tungsten deposition, then lifted out of the substrate using the probe, and finally attached via tungsten deposition to a four-post Omniprobe FIB grid (Ted Pella) for thinning. Different gallium ion beams of varying current were aimed at the micro-samples in order to first separate them from the probe, and then, mill these micro-samples to ~100 nm thick cross sections. Then, the FIB grid mounted on a FIB sample holder was removed from the FIB-SEM system, and, owing to the compatibility of the FIB and TEM sample holders, inserted directly into a Hitachi H-9500 high resolution transmission electron microscope (TEM) for imaging of the thinned Al

particles. Two Al microparticles were FIB-milled and TEM-imaged. Both particle cross sections revealed the grain structure.

Figure 1 shows a series of images that illustrates thinning of Al microparticle using FIB. First, an individual Al particle (~10 µm diameter) was selected for thinning (Fig. 1a). Next, a layer of carbon was deposited on the particle followed by a tungsten layer deposition (Fig. 1b). These layers serve as a protective barrier to the particle from the gallium ion beam damage. Various high current gallium ion beams were used to prepare ~5 µm thick Al particle slice (micro-sample), and subsequently, dig a trench around the micro-sample to free it from the substrate (Fig. 1c). The micro-sample was picked up by a tungsten probe and attached to a posted FIB grid (Fig. 1d). Finally, the micro-sample was milled to an electron-transparent TEM lamella with thickness of ~100 nm (Fig. 1e-f) using different gallium ion beams which varied in current value. Once the particle was thinned to ~100 nm, the FIB grid was transferred to a TEM. Results from the TEM analysis are shown in the results section.
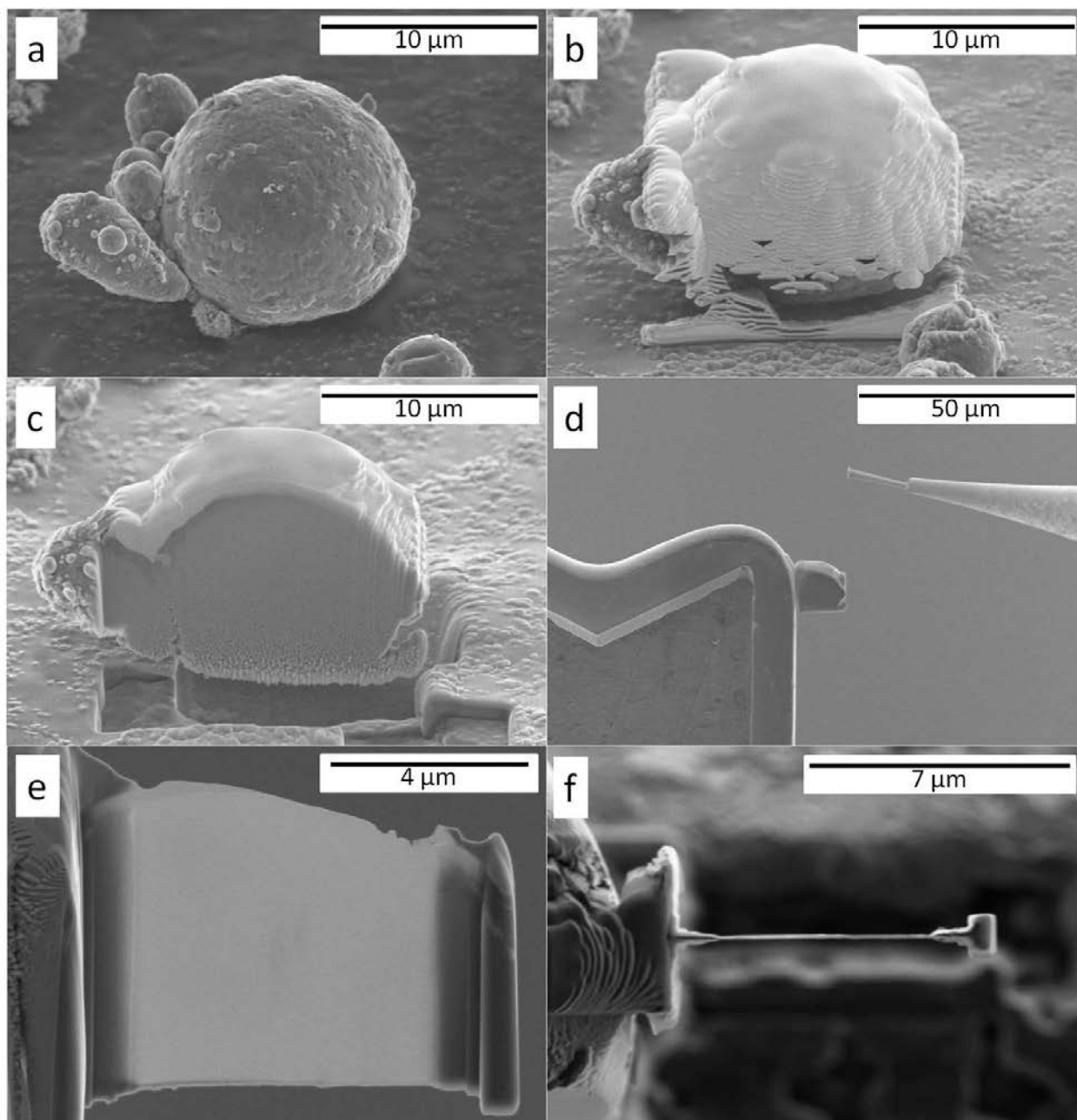
Figure 1. SEM and FIB visualization of thinning of Al microparticle: SEM images of (a) starting Al microparticle, (b) Al microparticle coated with carbon and tungsten films, (c) ~5 µm thick Al particle slice (micro-sample), (d) starting micro-sample attached to the FIB grid SEM (e) and FIB secondary electron (f) images of the micro-sample thinned to ~100 nm thickness.

Results and Discussion

Figure 2a shows the grain structure in the thinned Al particle as imaged by TEM. High-resolution TEM images from several different grains illustrated in **Fig. 2a** were acquired and are presented in **Fig. 2b-g**. The single crystal structure of an individual grain can be inferred from these images, which show a lattice spacing of 0.23 nm, in good agreement with the spacing of the (111) crystal planes of Al. Furthermore, the random orientation of the imaged Al lattice illustrated in **Fig. 2b-g** confirms that these are, in fact, images of individual grains and not an artifact from sample preparation. Overall, data shown in **Fig. 2** indicates the polycrystalline nature of Al microparticles investigated in this study, and interestingly all are large grains (i.e., > 100 nm).
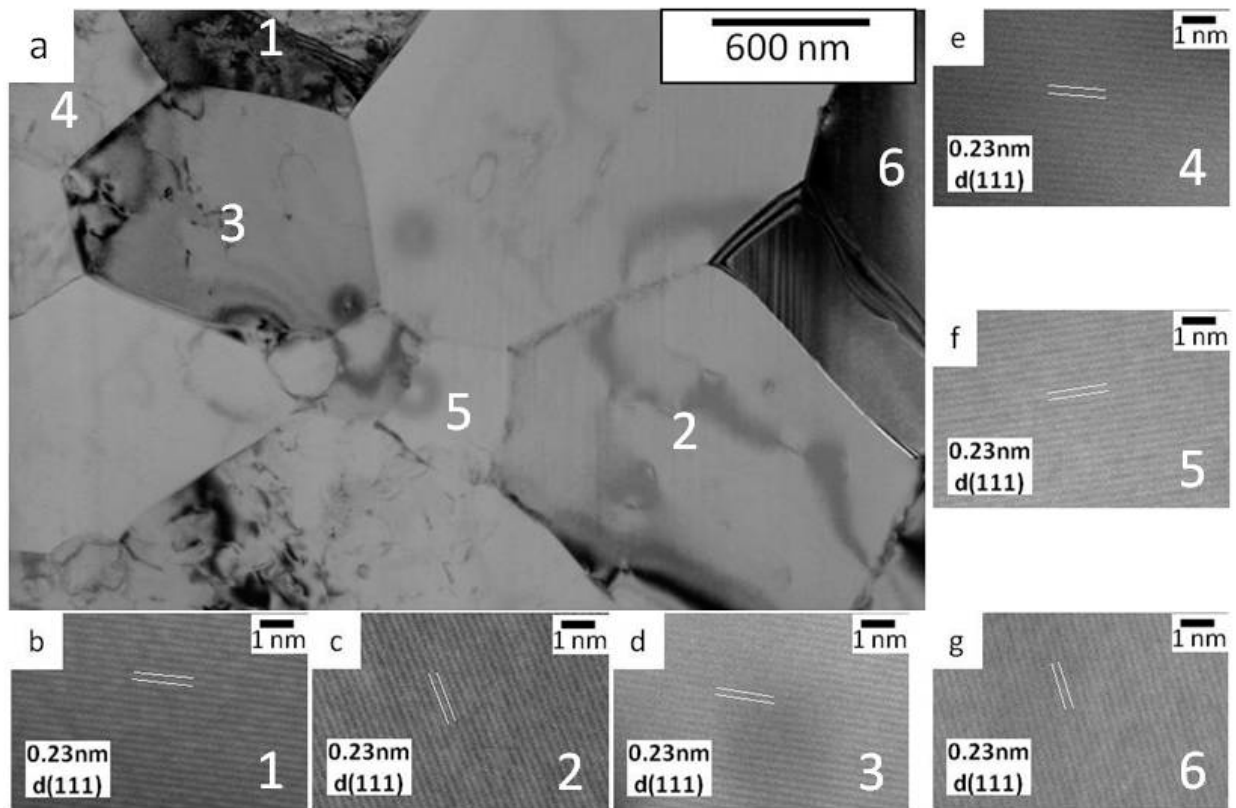

Figure 2. TEM visualization of the grain structure in a thinned cross section (~100 nm thick) of Al particle with starting diameter of ~10 µm: (a) TEM image acquired at 8,000x magnification shows the grain structure of Al particle, and (b)-(g) high-resolution TEM images acquired at 1,500,000x magnification illustrate lattice orientation for several grains shown in (a). The lattice

spacing of 0.23 nm in (b)-(g) corresponds to the spacing of the (111) crystal planes of Al. The grain lattice orientations shown in (b)-(g) correspond to the grains numbered 1-6 in (a), respectively.

Average strain values were calculated by performing a count weighted average of the distributions for dilatational strain shown in **Fig. S3** and are shown in **Table 1**. **Figure S4** also shows the distributions for average peak width. The low annealing temperatures and untreated data presented in **Figs. S3 and S4** are from synchrotron XRD measurements originally reported in [20, 25]. It is important to note that thermal treatments are identified by their annealing temperature in °C (i.e., 100, 200, 300 °C) and cooling rate is identified as *s* (slow cool for 0.007 to 0.014 K·s^{-1}) or *f* (fast cool for 0.13 to 0.38 K·s^{-1}). The 300s and 300f strain values reported in Table 1 and Figs. S3 and S4 are new and have not been previously reported for aging to 28 days. The strain values for the treated Al particles represent the change in volume from the untreated case. The strain values for Al particles annealed and quenched to 100*s* and 200*s* °C are within instrument resolution and are considered unchanged from the untreated Al powder. Aluminum particles that were annealed to 300*f* and 300*s* °C (both fast and slow quench rates) show a strain increase that is outside of the instrument resolution. From the untreated case, 300*s* increased by 5687% and 300*f* increased by 6053% as shown in **Table 1**. The strain increase from the untreated Al particles and those annealed to 100 and 200 °C are significantly smaller than particles annealed to 300 °C (i.e., the difference in strain is larger than the instrument resolution).

Figure S4 shows the average diffraction peak width that characterizes heterogeneity of stresses within a particle. Heat treatment causes an increase in the magnitude of stress heterogeneity. According to linear elastic theory, the stress heterogeneity should be proportional to the applied or average stress, thus **Figs. S3 and S4** are qualitatively consistent. The distributions in **Figs. S3 and S4** for the untreated Al and 100-200 were reported in [20] and

reproduced here for ease of comparison to the 300*f* and 300*s* case that are consistent with synchrotron XRD measurements reported previously but for different aging times [25].

Normalized flame speed values for each sample are shown in **Fig. 3**. The flame speed is normalized to the untreated flame speed such that a percent increase is apparent. Samples annealed to 100 and 200 °C show flame speed increases of only 1-5% from the untreated case. This increase is within measurement uncertainty thus considered unchanged. Samples annealed to 300 °C resulted in a 19% increase for the slow quenching rate and 24% increase for the fast quenching rate. The uncertainty in the flame speed results in an overlap for both fast and slow cooled samples such that flame speed does not increase significantly from quenching environment for these particular treatment parameters. Explicitly, for both cooling rates the flame speed difference is negligible but measurably higher for the highest temperature annealing case.
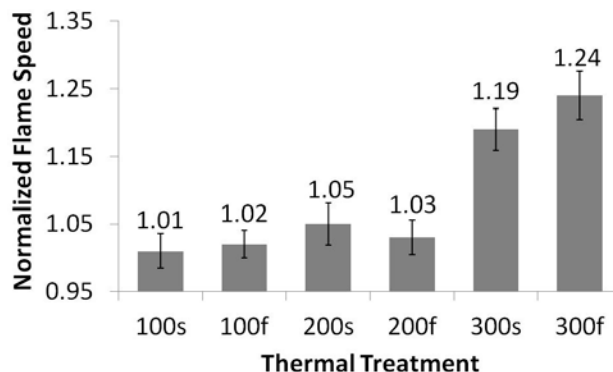

Figure 3. Normalized flame speed values for all thermal treatments. Each data point is designated by the annealing temperature (i.e., 100, 200 or 300 °C) and cooling rate (i.e. *s*=slow or *f* =fast).

When comparing strain values with flame speed, both trends are consistent: increased strain correlates with increased flame speed. This observation implies that activating a difference in strain also affects reactivity, at least as observed with flame speeds. Results for

grain microstructure (see Fig. 2) show relatively large grains, such that annealing and quenching will influence particle hardness [21]. For polycrystalline materials, like the Al powder in this study (see **Fig. 2**), plastic deformation is a viable response to thermal treatment. Bachmeier and Pippan [21] showed the hardness response for micron-scale Al powder (1.3 and 90 average μm) as a function of annealing temperature. They found minimal hardness changes for annealing temperatures below 200 °C followed by a decrease in hardness for higher annealing temperatures (i.e., >200-500 °C). They measured grain size by XRD for each Al powder and found increased grain sizes for samples annealed above 200 °C. Their results indicate that increased strain with annealing and quenching also increases grain size and decreases particle hardness. It is possible that the increase in strain is caused by a combination of both elastic and plastic changes in Al particles due to Al core/Al_2O_3 shell interactions and grain growth, respectively. Results shown here suggest that the elastic contribution to strain increase may be small because cooling rate plays a small role in the measured strain difference and flame speed increase. Also, reduced particle hardness may promote flame speeds by facilitating inter-particle collisions that produce enough energy to promote ignition and propagation. Additionally, grain growth may improve diffusion by allowing increased molecular motion to occur at the shell-core interface. A final possibility is that cracks that form in the shell from thermal stress during heat treatment may not heal fully or may have boundaries that allow increased oxygen diffusion through the shells into the aluminum particle core. The parameter of hardness is a new consideration for enhancing Al particle reactivity and further investigation is needed, but results shown here and by Backmeier and Pippan [21] suggest there is a feasible connection between reduced hardness and increased flame speed.

Conclusion

For cooling rates ranging from 0.007 to 0.38 K s^{-1} these experiments make clear that cooling rate has little effect on Al particle strain manipulation and subsequent reactivity measured in terms of flame speed. Strain increases with annealing temperature above 200 $^{\circ}$C, and varies only slightly with cooling rate. This new information confirms that the dominant mechanism in mechanical change occurs at an elevated anneal temperature (i.e., > 200 $^{\circ}$C), and is independent of the cooling rate regime studied here. The strain variations from 0.15 x 10^{-5} (for untreated Al powder) to 9. 23 x10^{-5} (for 300 $^{\circ}$C annealing) have a distinct effect on flame speeds: increasing flame speed by 21$\pm$2% upon annealing to 300 $^{\circ}$C. The precise mechanism controlling reactivity is not clear but the results shown here and in the literature for similar particles indicate a correlation between Al particle increased dilatational strain, increased grain size, decreased hardness and increased flame speed. Critical temperature for mechanical change is consistent with literature and suggests mechanical change is partly induced by grain growth. Focused ion beam (FIB) preparation and transmission electron microscope (TEM) imaging of a thin (i.e., ~100 nm) slice of a 10 µm diameter Al particle show clear images of the grain structure within the core of an Al particle. All grains are on the order of 100 nm dimensions. This supports the theory that thermal treatment of micron-scale Al powder results in plastic as well as elastic deformation, resulting in altered mechanical properties that affect reactivity.

Acknowledgments

References

[1]   M. Shigeta, T. Watanabe, Growth model of binary alloy nanopowders for thermal plasma synthesis, J. Appl. Phys. 108 (2010).

[2]   S. Deevi, V. Sikka, C. Swindeman, Application of reaction synthesis principles to thermal spray coatings, J. Mater. Chem. A. 32 (1997) 3315–3325.

[3]   C.L. Yeh, Y.S. Huang, Thermite reduction of Ta2O5/SiO2 powder mixtures for combustion synthesis of Ta-based silicides, J. Alloy. Compd. 509 (2011) 6302–6306.

[4]   M. Iordachescu, D. Iordachescu, E. Scutelnicu, J. Ruiz-Hervias, A. Valiente, L. Caballero, Influence of heating source position and dilution rate in achieving overmatched dissimilar welded joints, Sci. Technol. Weld. Join. 15 (2010) 378–385.

[5]   Y. Chen, F.V. Lawrence, C.P.L. Barkan, J.A. Dantzig, Heat transfer modelling of rail thermite welding, Proc. Inst. Mech. Eng., Part F. 223 (2006) 207–217.

[6]   C. Crane, M.L. Pantoya, Dunn, Infrared measurements of energy transfer from energetic materials to steel substrates, Int. J. Therm. Sci. 49 (2010) 1877–1885.

[7]   O.G. Cervantes, J.D. Kuntz, A.E. Gash, Z. a. Munir, Activation energy of tantalum–tungsten oxide thermite reactions, Combust. Flame. 158 (2011) 117–122. doi:10.1016/j.combustflame.2010.07.023.

[8]   V.I. Levitas, B.W. Asay, S.F. Son, M. Pantoya, Melt dispersion mechanism for fast reaction of nanothermites, Appl. Phys. Lett. 89 (2006) 071909. doi:10.1063/1.2335362.

[9]   V.I. Levitas, B.W. Asay, S.F. Son, M. Pantoya, Mechanochemical mechanism for fast reaction of metastable intermolecular composites based on dispersion of liquid metal, J. Appl. Phys. 101 (2007) 083524. doi:10.1063/1.2720182.

[10]   M.A. Trunov, M. Schooenitz, E.L. Dreizin, Effect of polymorphic phase transformations in the alumina layer on ignition of aluminum particles, Combust. Theory Model. 10 (2006) 603–623.

[11]   E.L. Dreizin, On the mechanism of asymmetric aluminum particle combustion, Combust. Flame. 117 (1999) 841–850.

[12]   M. a Trunov, S.M. Umbrajkar, M. Schoenitz, J.T. Mang, E.L. Dreizin, Oxidation and melting of aluminum nanopowders., J. Phys. Chem. B. 110 (2006) 13094–9. doi:10.1021/jp0614188.

[13]   K.T. Sullivan, N.W. Piekiel, C. Wu, S. Chowdhury, S.T. Kelly, T.C. Hufnagel, et al., Reactive sintering: An important component in the combustion of nanocomposite thermites, Combust. Flame. 159 (2012) 2–15. doi:10.1016/j.combustflame.2011.07.015.

[14]   A. Rai, K. Park, L. Zhou, M.R. Zachariah, Understanding the mechanism of aluminum nanoparticle oxidation, Combust. Theory Model. 10 (2006) 603–623.

[15]   K. Sullivan, M.R. Zachariah, Simultaneous pressure and optical measurements of nanoaluminum thermites: investigating the reaction mechanism, J. Propuls. Power. 26 (2010) 467–472.

[16]   P. Chakraborty, M.R. Zachariah, Do nanoenergetic particles remain nano-sized during combustion?, Combust. Flame. 161 (2014) 1408–1416. doi:10.1016/j.combustflame.2013.10.017.

[17]   V.I. Levitas, B. Dikici, M.L. Pantoya, Toward design of the pre-stressed nano- and microscale aluminum particles covered by oxide shell, Combust. Flame. 158 (2011) 1413–1417. doi:10.1016/j.combustflame.2010.12.002.

[18]   V.I. Levitas, J. McCollum, M. Pantoya, Pre-Stressing Micron-Scale Aluminum Core-Shell Particles to Improve Reactivity, Sci. Rep. 5 (2015) 7879. doi:10.1038/srep07879.

[19]   A. Ermoline, D. Stamatis, E.L. Dreizin, Low-temperature exothermic reactions in fully dense Al-CuO nanocomposites, Thermochim. Acta. 527 (2012) 52–58.

[20]   J. McCollum, M.L. Pantoya, N. Tamura, Improving Aluminum Particle Reactivity by Annealing and Quenching Treatments: Synchrotron X-ray Diffraction Analysis of Strain, Acta Mater. In Press (2015).

[21]   A. Bachmaier, R. Pippan, Effect of oxide particles on the stabilization and final microstructure in aluminium, Mater. Sci. Eng. A. 528 (2011) 7589–7595. doi:10.1016/j.msea.2011.06.071.

[22]   H. Abdoli, M. Ghanbari, S. Baghshahi, Thermal stability of nanostructured aluminum powder synthesized by high-energy milling, Mater. Sci. Eng. A. 528 (2011) 6702–6707. doi:10.1016/j.msea.2011.05.057.

[23]   M. Kunz, N. Tamura, K. Chen, A.A. MacDowell, R.S. Celestre, M.M. Church, et al., A dedicated superbend X-ray microdiffraction beamline for materials, geo-, and environmental sciences at the advanced light source., Rev. Sci. Instrum. 80 (2009) 035108.

[24]   N. Tamura, XMAS: a versatile tool for analyzing syncrotron x-ray microdiffraction data. Microdiffraction analysis local and near surface hierarchical organization of defects, London, 2013.

[25]   B.S.M. Claudio L. De Castro, Nanoparticles from Mechanical Attrition, Synth. Funct. Surf. Treat. Nanoparticles. (2002) 1–14.

[26]   Levitas, V.I., McCollum, J., Pantoya, M.L., Tamura, N., Stress Relaxation in Pre-Stressed
       Aluminum Core-Shell Particles: X-Ray Diffration Study, Modeling, and Improved
       Reactivity, Comustion and Flame 170, (2016) 30-36.

Table 1. Average dilatational strain values, percent increase in strain and percent increase in flame speed for all thermal treatments. Each sample is designated by the annealing temperature (i.e., 100, 200 or 300 °C) and cooling rate (i.e., *s* (slow) or *f* (fast)).

Sample	Average Strain	Strain % Increase	Flame Speed % Increase
Untreated	0.15×10^{-5}	---	---
100s	Not Measured	---	$1 \pm 2\%$
100f	0.87×10^{-5}	---	$2 \pm 2\%$
200s	Not Measured	---	$5 \pm 3\%$
200f	0.86×10^{-5}	---	$3 \pm 2\%$
300s	8.68×10^{-5}	5687%	$19 \pm 3\%$
300f	9.23×10^{-5}	6053%	$24 \pm 4\%$